

# Environmental magnetism assessing coastal deoxygenation history in the northern Baltic Sea during Holocene thermal maximum from a high time resolution sedimentary sequence

Sonja Silvennoinen<sup>1)\*</sup>, Johanna Salminen<sup>1)2)</sup>, Seija Kultti<sup>1)</sup> and Niko Putkinen<sup>2)</sup>

<sup>1)</sup> Department of Geosciences and Geography, University of Helsinki, P.O. Box 64, FI-00014, Finland

<sup>2)</sup> Geological Survey of Finland, FI-67101, Kokkola, Finland

\*corresponding author's e-mail: [sonja.silvennoinen@helsinki.fi](mailto:sonja.silvennoinen@helsinki.fi)

Received 15 May 2024, final version received 28 Jan. 2025, accepted 28 Jan. 2025

Silvennoinen S., Salminen J., Kultti S. & Putkinen N. 2025: Environmental magnetism assessing coastal deoxygenation history in the northern Baltic Sea during Holocene thermal maximum from a high time resolution sedimentary sequence. *Boreal Env. Res.* 30: 55–76.

The central Baltic Sea has one of the largest hypoxic zones in the world, and during the past decades, increasing hypoxic conditions have also been observed in the coastal zone. While the Holocene development of repeated hypoxia in the Baltic Sea basin is well studied in multiple central and southern Baltic deep-sea cores, less is known about the development of the coastal zone during the Holocene thermal maximum (HTM). Understanding the coastal hypoxia during HTM is topical, providing an analogy for assessing future development of hypoxia in a warming climate. A high resolution (average sediment accumulation rate 0.65 cm/a) ~40-m long sediment core from coastal eastern Bothnian Sea (Kurikka, S. Ostrobothnia, Finland) was analysed with lithological and environmental magnetic methods. This core covers local deglaciation and basin evolution from a freshwater to brackish phase until isolation from the sea (~10.6–4.3 ka). The study site featured freshwater offshore conditions that transformed into a brackish coastal estuary environment with ongoing shallowing. Environmental magnetic methods and occurrence of magnetic mineral greigite (Fe<sub>3</sub>O<sub>4</sub>) was used to assess oxygen conditions along the sediment sequence. Magnetite was found in Ancylus lake sediments, while both greigite and magnetite was found in Littorina Sea deposits. Greigite was identified as SD-sized and authigenic with signs of formation within the sulphidic zone, contrasting the central Baltic Littorina Sea sediments, where bacterial greigite has previously been found. Results indicate that deoxygenation was common, but frequently interrupted during the HTM in the shallowing coastal Bothnian Sea. Two multicentennial predominantly hypoxic periods and two intensive decadal hypoxic events were observed with more regular oxic conditions in between. However, the interpreted greigite concentrations were variable within the hypoxic interval, suggesting unstable oxygen conditions and perennial trends in deoxygenation intensity. The pattern seen in Kurikka record corresponds with the description of a multicentennial nature of hypoxia variability in the Baltic Sea with oscillating intensity, suggesting basin-wide regularity and common drivers of hypoxia.

## Introduction

Bottom water oxygen depletion, hypoxia ( $O_2$  concentration  $< 2 \text{ mg L}^{-1}$ ) causes severe ecosystem disturbance in the water basin and sulphide sediment deposition in environments like the present-day Baltic and Black Sea (Diaz and Rosenberg 2008, Middelburg and Levin 2009). The hypoxic formation environments of sulphide sediments are a growing global concern (Breitburg *et al.* 2018), and when uplifted above the sea level, these sediments become acid sulphate soils known to cause societal, financial, and environmental harm (Fältmarsch *et al.* 2008). Both natural and anthropogenic factors cause present day hypoxia in the Baltic Sea basin (Zillén *et al.* 2008). In 2019, the central Baltic Sea was determined to contain one of the largest hypoxic zones in the world (Fennel and Testa 2019), and during the past decades, increasing hypoxic conditions have been obtained also in the coastal zone (Conley *et al.* 2011). Besides restricted water circulation, coastal hypoxia is caused by nutrient loads from urban and agricultural sources driving phytoplankton growth and increased oxygen consumption in the Swedish and Finnish archipelagos (Conley *et al.* 2011). By contrast, the deep basins below the halocline of the Baltic Sea are permanently stratified (Conley *et al.* 2009).

Repeated natural hypoxic intervals have been linked to warmer than present conditions in the Baltic Sea Basin during the Holocene thermal maximum (HTM, ca. 8–4 ka) and Medieval Climate Anomaly (Zillén *et al.* 2008). While the Holocene development of repeated hypoxia is well studied in multiple central and southern Baltic deep-sea cores, a limited number of studies have focused on the development of Baltic Sea coastal hypoxia (Ning *et al.* 2016, van Helmond *et al.* 2017, Dijkstra *et al.* 2018, Jokinen *et al.* 2018). Only some of these extend across the HTM period, leaving the early HTM understudied. Moreover, temporal resolution enabling detailed examination on the multiannual development of hypoxia is lacking in both coastal and deep-sea sediment studies (Jilbert *et al.* 2021). Understanding the driving forces for coastal hypoxia during HTM is topical, providing an analogy for assessing future development of hypoxia in a warming climate.

Hypoxia alters also the seafloor redox conditions. Diagenesis is driven by degradation of organic matter, where different electron donors are used in a subsequent order (Froelich *et al.* 1979), creating diagenetic / chemical zones. Diagenetic environments with different redox levels produce specific mineral assemblages with distinctive magnetic properties that can be differentiated using environmental magnetic methods (Roberts *et al.* 2018). A magnetic mineral greigite ( $Fe_3S_4$ ) can form under anoxic conditions in sulphidic and methanogenic redox zones (Roberts *et al.* 2018). Therefore, the presence and characteristics of greigite in sediments offer a novel proxy for anoxia and other environmental processes (Li *et al.* 2019, Ebert *et al.* 2020, Chen *et al.* 2021). Greigite is formed either authigenically or by magnetotactic bacteria in various grain sizes. Bacterial greigite has usually a very narrow size distribution, while authigenic greigite can present in a wider size range (Roberts *et al.* 2011). Yet, the formation and magnetic characteristics of greigite are still actively explored (Roberts *et al.* 2011, Roberts *et al.* 2018, Li *et al.* 2019). Greigite has been identified from deep Baltic Sea sediments (e.g., Sohlenius 1996, Kortekaas 2007, Lougheed *et al.* 2012, Reinholdsson *et al.* 2013), but the formation pathways are still under debate.

Recent studies have brought light to the complexity of the Finnish Ostrobothnian Quaternary stratigraphy that ranges from early Weichselian sediments to the last deglaciation and subsequent aquatic deposition (Putkinen *et al.* 2020, Hall *et al.* 2021, Malinowski *et al.* 2023). The HTM alone has resulted in tens of meters of sulphide sediments, capturing the development of a shallowing coast. Here a ~40-m long sediment record with average accumulation rate of 0.65 cm/a from Kurikka, Southern Ostrobothnia, Finland is studied, providing a unique opportunity for reviewing the evolution of coastal deoxygenation in the northern Baltic Sea during the HTM. This study aims to: 1) construct the stratigraphy; 2) distinguish the magnetic minerals in the Kurikka sediment sequence; 3) distinguish the origins for the magnetic minerals and understand the diagenetic environment; and 4) study the patterns in the development of oxygen condition variability.

## Study site

The Bothnian Sea is a northern sub-basin of the Baltic Sea, divided from the central Baltic by a sill. The Bothnian Sea is a coastal basin with low salinity (~4–6 ‰), shallow waters and no current hypoxia, with multiple rivers feeding fresh water and terrestrial matter into the Sea. The Bothnian Sea region became ice-free ca 11.3–10.5 ka. After deglaciation, the Baltic Sea basin has experienced multiple freshwater and brackish phases. The water body of the lacustrine Ancylus phase following deglaciation in Bothnian Sea was well mixed and oxygenated (Sohlenius *et al.* 1996, Andrén *et al.* 2011, Warnock *et al.* 2018). The salinity of the Baltic Sea basin started to increase around 8 ka (Andrén *et al.* 2000a, Andrén *et al.* 2000b, Sohlenius *et al.* 2001, Berglund *et al.* 2005). The rise in salinity that marks the initiation of the Littorina Sea phase, was caused by the enabled contact with the Atlantic Ocean due to the rising eustatic sea level linked to the melting of ice sheets. By 7 ka the central Baltic Sea had a stratified water column and brackish water, with gradual and delayed increase in salinity further north (Sohlenius *et al.* 2001). Increased primary production across the Baltic Sea included with salinity stratification during the Holocene Thermal Maximum led to a +3-ka interval of hypoxia and in the deepest parts, periods of occasional euxinia (Sohlenius *et al.* 2001, Zillén *et al.* 2008, Jilbert *et al.* 2015). Intense hypoxic conditions during HTM have been observed in the northern sub-basins as well (Zillén *et al.* 2008, Jilbert *et al.* 2015, Häusler *et al.* 2017), but shallowing of the threshold between Bothnian Sea and the central Baltic Sea during mid- to late Littorina Sea phase hindered deep water exchange, leading to environmental separation of the northern and central Baltic Sea (Jilbert *et al.* 2015, Häusler *et al.* 2017). The salinity of the Baltic Sea decreased, and the oxygen conditions improved with the eustatic sea level rise ceasing at the onset of more humid and cold conditions (Gustafsson and Westman 2002). This is seen as the hypoxic zone diminishing in the central and northern Baltic Sea around 4 ka (Zillén *et al.* 2008, Jilbert and Slomp 2013, Jilbert *et al.* 2015, Häusler *et al.* 2017). In northern Baltic

Sea, signs of reduced salinity and climatic cooling is seen already before this (Tuovinen *et al.* 2008).

The study site (Fig. 1) in Kurikka, Southern Ostrobothnia, Finland is located in Kyrönjoki river valley, currently 58 m. a.s.l., on the eastern coast of Bothnian Sea. The site lies in a bedrock depression formed in an old rift valley associated with the preglacial river Eridanos (Gibbard and Lewin 2016, Hall *et al.* 2021). During the deglaciation of the Weichselian Late Glacial the area was at a lateral margin configuration between an interlobate area and an ice lobe (Boulton *et al.* 2001). Towards the end of the deglaciation, the lateral margin position shifted some kilometres, leaving a interlobate esker (Niemelä *et al.* 1993) and till-dominated marginal deposits later covered by fine basin sediments (Malinowski *et al.* 2023). The region became ice-free at approximately 10.6 ka ago (Stroeven *et al.* 2016) and submerged as a part of the Bothnian Sea. Since the local deglaciation, the study site has accumulated ~40 meters of sediments from deglaciation and the last Baltic Sea stages until isolation from the sea. During this time, the sedimentation environment has changed due to relative sea level change. Immediately after deglaciation, during the lacustrine Ancylus phase, the water depth on the study area was approximately ~190 m (see Fig. S1 in Supplementary Information), and with an estimated distance to the shore of ~70 km (Fig. 1; shoreline shown in light yellow) the study area featured open-water conditions. With isostatic uplift causing regression, the water depth decreased to < 60 m in the beginning of the Littorina Sea phase, turning the study site into an archipelago setting and finally into an estuary-type system, connected to the river Kyrönjoki (Fig. 1; shoreline shown in light green). During this time, the study site featured a sheltered sedimentation environment with an island to the west providing shield from prevailing southwestern wind and wave action. The study site was supposedly closely linked to the Kyrönjoki river feeding fresh water and terrestrial matter into the bay. With increasing shallowing, the site was uplifted above sea level at ~4.5–4.3 ka ago (see Fig. S1 in Supplementary Information for relative shoreline displacement curve).

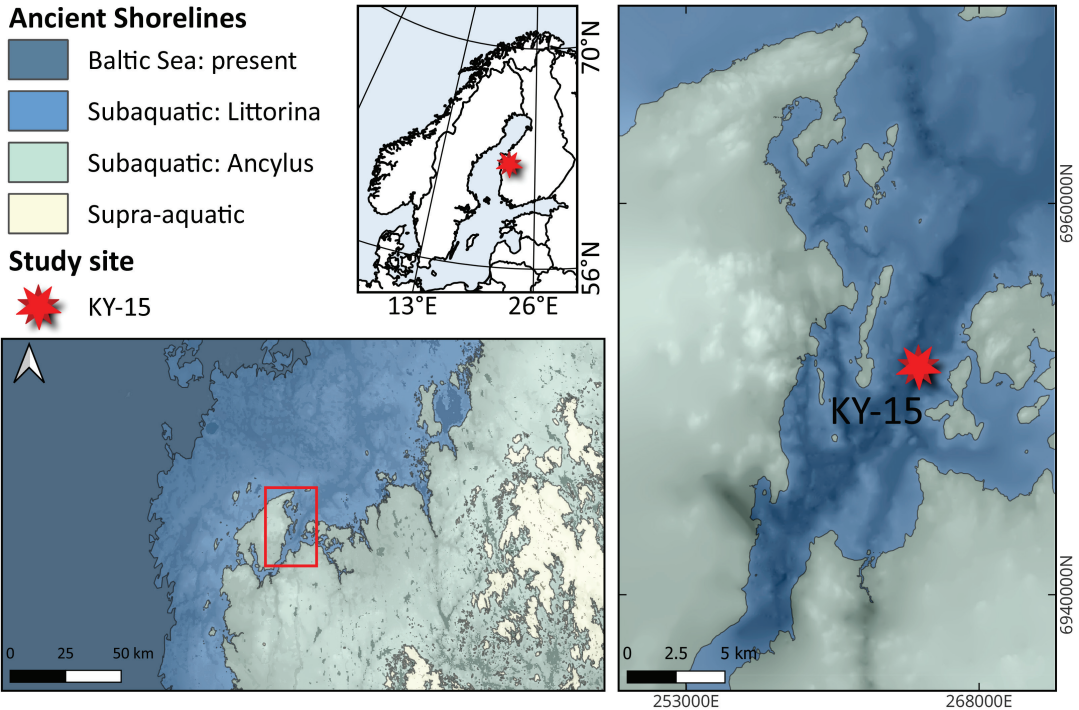


**Fig. 1.** Study site is located in Kurikka, Southern Ostrobothnia, Finland. Due to isostatic uplift, the shoreline has shifted across the Baltic Sea basin. During lacustrine Ancylus phase (subaquatic areas shown in light green and blues) the study site has been offshore, ca 70 km from the then coastline. During the later brackish Littorina Sea phase (subaquatic areas shown in blues), the study site was coastal, protected by a large island to the west. Darker areas indicate deeper bedrock topography and gives indication on the bathymetry of the sedimentation basin. Ancient shorelines (1:1 000 000 © Geological Survey of Finland); basemap on left: Bedrock surface (1:1 000 000 © Geological Survey of Finland); basemap on right: Kurikka Bedrock elevation model (Malinowski *et al.* 2023).

## Material and methods

The sediment core KY15 (0.5–41.6 m depth below surface) was retrieved from Kurikka, Southern Ostrobothnia, Finland (62.6204°N 22,4149°E, WGS84) in May 2019. The sediment core was drilled with a GM 200GT heavy-duty soil investigation drill rig as a continuous series of 1-m-long sections until 39 m depth until bedrock was reached with a 2-meter bedrock control. Preliminary visual interpretation of sediment was obtained during coring. The sections were sealed in plastic and stored in +6 °C at the University of Helsinki. Upon subsampling in 2019–2020, the sediments were split, trimmed, logged, and photographed section by section downcore at the University of Helsinki. Colour of sediment was determined using a Munsell colour chart. For sedimentological analysis, discrete subsamples were extracted on

equal intervals and upon lithological contacts into plastic bags and stored in +6 °C. Details on sampling are presented in Supplementary Information section S1 and Table S1.

The organic content was determined from subsamples by loss on ignition (LOI) (Dean 1974, Heiri *et al.* 2001) at Hellabs, University of Helsinki using a LECO TGA701 thermogravimetric analyser. For grain size analysis, subsamples were pretreated with 30% H<sub>2</sub>O<sub>2</sub>, 10% NaOH and 10% HCl (see details in Supplementary Information section S2). Before the analysis, 0.0134 M sodium pyrophosphate (Na<sub>4</sub>P<sub>2</sub>O<sub>7</sub>) was added as a dispersant and subsamples were treated with ultrasonic vibration for 60 seconds to avoid flocculation. Grain size distributions were analysed with a Malvern Mastersizer 2000 Laser Diffractometer at Hellabs. Due to the underestimation of the clay fraction by laser diffraction method (Konert

and Vandenberghe 1997), 6.3  $\mu\text{m}$  is used to represent the 2  $\mu\text{m}$  upper clay fraction boundary (Ramaswamy and Rao 2006).

Radiocarbon-AMS determinations (De Vries and Barendsen 1954, Tikkanen *et al.* 2004) of two terrestrial plant remains, one marine shell and four bulk sediment subsamples (see details in Table S1) were performed at the Laboratory of Chronology at the Finnish Museum of Natural History, University of Helsinki. The results were calibrated to the IntCal20 -calibration curve (Reimer *et al.* 2020) using OxCal calibration program version 4.4 (Bronk-Ramsey 2009) and are presented as years cal BP. The marine shell macrofossil age (depth 10.5 m) was calibrated without the marine reservoir correction due to the immediate proximity to the shore of the location, the reported dynamics in Baltic Sea reservoir ages (Lougheed *et al.* 2012) and better agreement with the over- and underlying terrestrial plant macro fossil dates. Due to the limited amount of datings, both age-depth model and estimations on sedimentation rates are tentative (see details in Supplementary Information section S3 and Fig. S2 for the age-depth model). The mean sedimentation rates are given rough estimates based on radiocarbon dates and presumed deglaciation and isolation times. Water depths during sedimentation were estimated from a tentative age-depth model and a relative shoreline displacement curve that was drawn based on nearby shoreline observations from ancient shoreline database (Geological survey of Finland), nearby isolation dating results from Eronen (1974), Glückert *et al.* (1993), Vuorela *et al.* (2009) and a radiocarbon date from this study (Table 1) (see details in Supplementary Information section S3 and Fig. S1 for the relative shoreline displacement curve).

For environmental magnetic measurements, 23 subsamples were collected from selected depths of units 2–4 in April 2021 at the University of Helsinki, by gently pushing 8  $\text{cm}^3$  plastic cubes into the fresh sediment surface where oxidized sediment was removed before sampling. Environmental magnetic measurements apart from thermomagnetic measurements were carried out in the Solid Earth Geophysics Laboratory of the University of Helsinki. Used methods and acquisition steps are presented in Table S2 in Supplementary Information. Magnetic susceptibility ( $\kappa$ ) was measured directly from the surface of the plastic wrapped split cores with a handheld SM-30 magnetic susceptibility meter (ZH Instruments, 8 kHz frequency) on two measurement intervals (see Table S1 in Supplementary Information). Mass-specific magnetic susceptibility ( $\chi_{\text{sp}}$ ,  $\chi_{\text{hf}}$ ) of discrete 8  $\text{cm}^3$  cubic subsamples were measured with a ZH Instruments SM105 magnetic susceptibility meter with two frequencies (320  $\text{Am}^{-1}$ ;  $\chi_{\text{hf}}$  500 Hz,  $\chi_{\text{hf}}$  8000 Hz). Frequency dependent susceptibility ( $\chi_{\text{fd}}$  %) was calculated as a percentage loss of magnetic susceptibility following Dearing *et al.* (1996) (see Supplementary Information section S4).

Natural remanent magnetization (NRM) of each subsample was measured and demagnetized with 755-R single-sample 2G-SQUID magnetometer. Subsamples were step-wisely demagnetized with alternating field (AF) in 12 steps (up to 100 mT) using an automated 2G-SQUID magnetometer (see Table S2). The demagnetizing field needed to halve the NRM, i.e. median destructive field of NRM ( $\text{MDF}_{\text{NRM}}$ ), was obtained.

Anhysteretic remanent magnetization (ARM) was imparted using 100 mT peak alternating field (AF) and a constant 0.1 mT direct field

**Table 1.** AMS-radiocarbon dating results.

Unit	Depth m	Material	Radiocarbon age yr BP	Calibrated mean age cal BP $\pm 1\text{s}$	Laboratory code
U5B	0.6	Bulk sediment (gyttja)	3879 $\pm$ 19	4322 $\pm$ 53	Hela-5145
U5B	0.91*	Bulk sediment (silt)	16360 $\pm$ 50	redeposited	Hela-5144
U4	9.31	Plant remains	5657 $\pm$ 33	6437 $\pm$ 40	Hela-4696
U4	10.50	Marine shell	5881 $\pm$ 34	6703 $\pm$ 38	Hela-4699
U4	16.50	Plant remains	6495 $\pm$ 38	7398 $\pm$ 45	Hela-4698
U1	32.97*	Bulk sediment (silt)	30740 $\pm$ 140	redeposited	Hela-5131
U1	35.20*	Bulk sediment (silt)	30000 $\pm$ 130	redeposited	Hela-5130

\* Interpreted as redeposited material, rejected from the age-depth model

along z-axis with AGICO LDA-3A AF-demagnetizer and AMU-1A ARM magnetizer. ARM of the subsamples was measured and demagnetized stepwise with the 2G SQUID. The susceptibility of ARM ( $\chi_{\text{ARM}}$ ) was calculated for measured ARM values following Evans and Heller (2003) (see Supplementary Information section S4).

Rotational Remanent Magnetization (RRM) (Stober and Thompson 1979a, b, Stephenson 1980a, b, Snowball 1997b) was imparted with a Molspin triple mu-metal shielded AF demagnetizer, which operates at a frequency of 50 Hz and at a maximum AF of 100 mT. Subsamples were at first demagnetized with 2G SQUID magnetometer in a static position along three orthogonal axes (X, Y and Z) in a peak AF of 150mT and the residual magnetization was measured following Snowball (1997b). RRM was then induced by rotating subsamples around their -Z-axis at frequency of 5 rps, perpendicular to the 100 mT alternating field (see details in Supplementary Information section S4 and Fig. S3). Imparted remanence along -Z-axis was measured with 2G SQUID magnetometer. After that the process was repeated, but with the rotation around their +Z-axis following Reinholdsson *et al.* (2013). The final RRM value was calculated as the mean of the two measurements. A positive RRM is acquired if the magnetization is parallel to the rotation vector and negative if it is acquired anti-parallel (Fig. S3 in Supplementary Information). The effective gyro field ( $B_g$ ) was calculated following Snowball (1997b) as the ratio of the absolute value of RRM to ARM, multiplied by the strength of the DC bias field used to induce the ARM (see Supplementary Information section S4).

Isothermal remanent magnetization (IRM) along +Z-axis was imparted with the MMPM 10 pulse magnetizer at a field of 3T, and the produced saturation isothermal remanent magnetization (SIRM) was measured with a 2G SQUID magnetometer. Then the subsamples were magnetized in a reversed field of -100 mT with a MMPM 10 and the remanence was measured with a 2G SQUID magnetometer. S-ratio was calculated following Reinholdsson *et al.* (2013) and Stober and Thompson (1979b) as  $(\text{IRM}_{-0.1\text{T}}/\text{IRM}_{3\text{T}})$ . All subsamples were then demagnetized in same steps as NRM.

Temperature dependence of low-field magnetic susceptibility was measured from -192°C to ~700°C followed by cooling back to room temperature. Subsamples were measured with a AGICO MFKA-1A kappabridge (200 A/m, 976 Hz) at the Geophysical Laboratory of the Geological Survey of Finland and analysed with Cureval 8.0.2. High-temperature measurements were run in argon as reasoned by Muxworthy *et al.* (2023).

## Results and interpretations

### Radiocarbon dating of sediment record

AMS-radiocarbon dating results are presented in Table 1. Mean sedimentation rate estimated from local deglaciation (Stroeven *et al.* 2016) and isolation (this study) times gives the sediment succession an average temporal resolution across the sedimentary record of 1.5 a/cm. The age-depth model (Fig. S2 in Supplementary Information) is tentative due to limited dating results.

The age determination from depth 0.6 m was taken from post-isolation fine detritus gyttja, and the age represents minimum isolation time for the sediment sequence. Ages from depths 0.91 m, 32.97 m and 35.2 m are older than deglaciation in the area and are interpreted as reworked and redeposited material, rejected from the age-depth model.

### Sediment stratigraphy of Kurikka sediment core

The sediment succession was divided into five lithological units according to physical properties (lithology, organic content, grain size and magnetic susceptibility). The lithology of each unit is described below in detail from bottom to top and summarized along with physical properties in Table 2 and Fig. 2.

The basal KY15-U1 unit (sediment depth below core surface 41–33 m) features light grey sands mixed with heavily deformed dark grey coarse silt and very light coarse sand interbeds of varying thickness (typically 2–5 mm, with distance from one silt bed to the next 15–20 cm).

Approximately eight sets are counted from one silt bed to the next. The grain size of the sediment fines upward until the sandy sediment is changed abruptly at 35.3 m to a rhythmic coarse silt. Individual varves are separated by fine sediment laminae and shift from irregular and deformed ~5 cm thick beds to more regular and slightly thinner ones, totalling to ~30–40 couplets. The unit is characterized with low organic content and high variability in grain size and magnetic susceptibility (Fig. 2) corresponding to ice frontal sedimentation. The bulk sediment radiocarbon dates (35–30 ka; Table 1) corresponding to Marine Isotope Stage (MIS) 3 show, that the material is reworked and redeposited sediment of glaciogenic origin. The unit is interpreted to represent local deglaciation with sandy glacial outwash connected to esker formation and with a distancing glacier front, glaciolacustrine rhythmites.

In the unit KY15-U2 (33–20.9 m), the rhythmite from U1 passes within ~5 cm to greenish grey silt, and with a couple odd couplets the rhythmic nature disappears. The greenish grey silt is mainly homogenous, with occasional coarser layers and very faint sulphide mottling, low organic content, and low magnetic suscep-

tibility. The organic content and the magnetic susceptibility remain constantly low within the unit (magnetic susceptibility:  $\sim 0.35 \pm 0.1 \times 10^{-3}$  (SI), LOI: 2–2.5%). The lithology corresponds to lacustrine *Ancylus* phase sediments from other Baltic Sea sediment cores (Winterhalter 1992). The low organic content and magnetic susceptibility indicate oligotrophic conditions (Sohlenius 1996) and the faint sulphide mottling is usually attributed to sulphide diffusing downward in the sediment column from overlying sediments (Sohlenius 1996).

In unit KY15-U3 (20.9–16 m) the lacustrine silts transition gradually within ~15 cm to sulphide banded gyttja silt with an increasing trend in organic content and magnetic susceptibility. Sulphide banding is mostly blurry / mottled. This unit is interpreted to represent the transition to Littorina Sea phase. Top 2.5 m of the unit feature homogenous greenish black silts.

In unit KY15-U4 (16–7 m) homogenous sulphide silt passes to into darker strongly laminated sulphide gyttja silt that feature occasionally varved behaviour, some coarser grained and some thin white laminae. Dense sulphide lamination is usually some millimetres thick. With highly varia-

**Table 2.** Sedimentary description of lithological units

Unit depth m	LOI %	d50 mm	$\kappa$ SI $10^{-3}$	Munsell colour	Estimated water depth m	Sediment description	Interpreted sedimentation environment
U5B 0.5–3.0	~1.0	35	$0.24 \pm 0.15$	Brown to grey	0–8	Fine detritus gyttja, sand with coarse beds, coarse massive silt	Beach deposition and isolation
U5A 3.0–7.0	1.2	16	$0.45 \pm 0.08$	Greenish dark grey	8–23	Sulphide banded silt	Littorina Sea, shallow
U4 7.0–16.0	2.6	10	$0.52 \pm 0.16$	Greenish black to black	23–45	Strongly laminated sulphide gyttja silt	Littorina Sea, coastal
U3 16.0–20.9	2.5	10	$0.50 \pm 0.12$	Greenish dark grey to very dark grey	45–50	Sulphide banded to homogenous gyttja silt	Littorina transition, coastal
U2 20.9–33.0	2.2	9	$0.36 \pm 0.08$	Greenish grey	50–170	Massive and faintly mottled silt	<i>Ancylus</i> lake, offshore
U1 33.0–39.0	<1.5	12 / 38	$1.24 \pm 0.56$	Light grey	~180	Fine sand to silt couplets	Deglaciation, proglacial basin
Observed at coring: 39.2–40.8						sand	Deglaciation, esker formation
40.8–41.6						fine sand	Deglaciation, esker formation

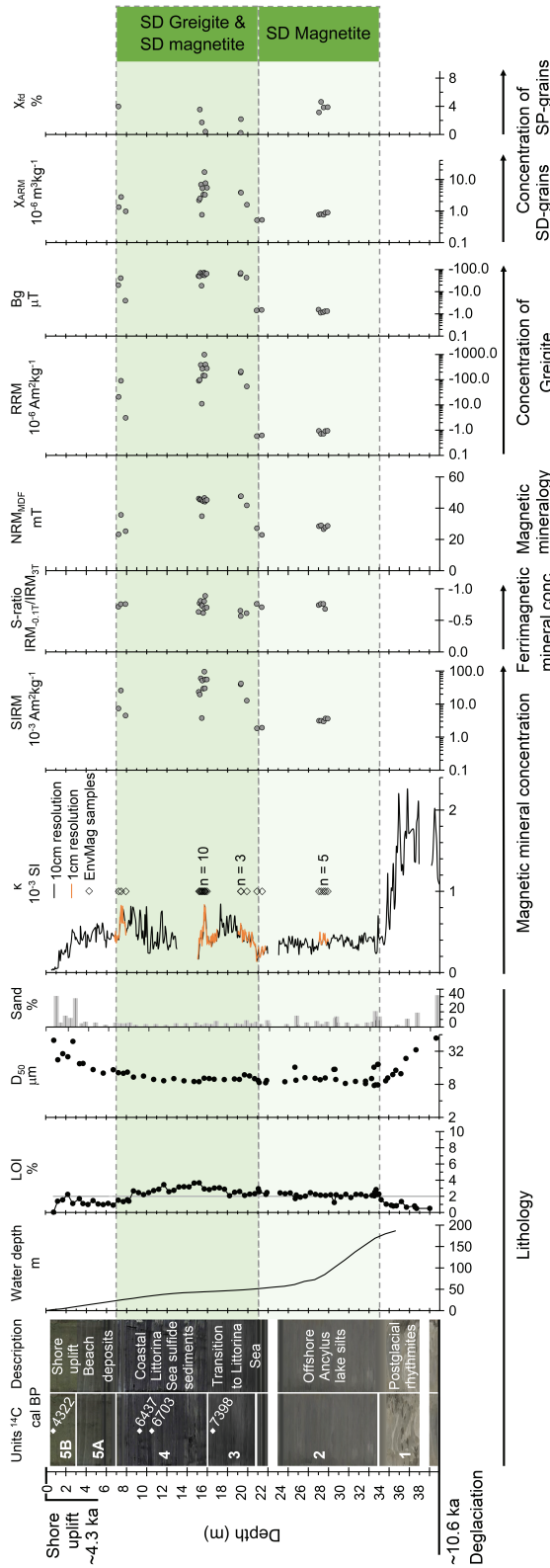


**Fig. 2.** Lithology, physical properties, and environmental magnetic characteristics from sediment core KY15 from Kurikka, Southern Ostrobothnia, Finland. From left to right: Lithological units with radiocarbon (<sup>14</sup>C) dates (cal BP), characteristic photos and short description of each lithology, estimated water depth (m), organic content (%) from Loss on Ignition, Grain size as D<sub>50</sub>-value (µm), sand content (%), magnetic susceptibility (k 10<sup>-3</sup> SI), Saturation Isothermal Magnetization (10<sup>-6</sup> Am<sup>2</sup> kg<sup>-1</sup>), S-ratio, NRM<sub>MDF</sub> (mT), Rotational Remanent Magnetization (10<sup>-6</sup> Am<sup>2</sup> kg<sup>-1</sup>), Biasing field (µT), Susceptibility of ARM (10<sup>-6</sup> m<sup>3</sup> kg<sup>-1</sup>), Frequency-dependent susceptibility (%) and the mineralogical interpretations (dark green boxes). Light green boxes in the background refer to the areas where mineralogical interpretations are assumed to apply. Magnetic susceptibility profile with 10 cm measurement point interval (black) and 1 cm measurement interval (orange). Core start and end ages inferred from estimates of local deglaciation and isolation. Note RRM and Bg inverted x-axis due to negative values.

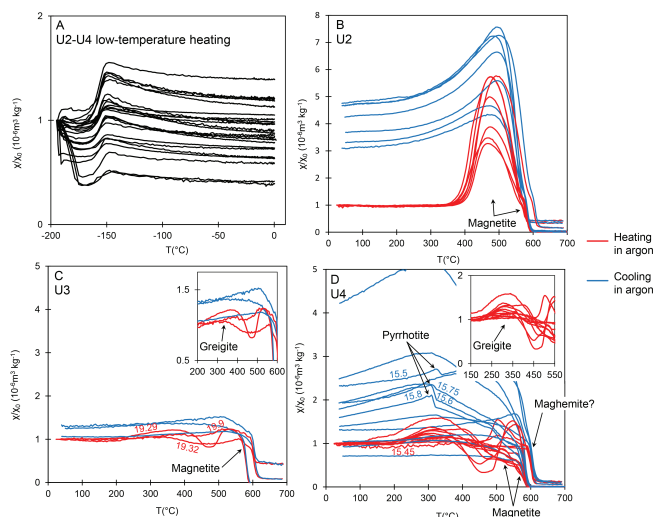


**Fig. 3.** Thermomagnetic behaviour of sub-samples divided between sedimentary units. Magnetic susceptibility on y-axis is normalized with the initial magnetic susceptibility. Interpretations of different magnetic susceptibility changes with arrows pointing to the decay area.

ble oscillating magnetic susceptibility and slightly elevated organic content, the sediments correspond to the marine *Littorina* Sea phase (Sohleinius 1996, Reinholdsson *et al.* 2013), supported by macrofossils dating to 6400 and 6700 cal BP (Table 1). Sulphide lamination transitions to faint and irregular from 11 m upward.

Unit KY15-U5 is divided into two sub-units. In sub-unit KY15-U5A (7–3 m), sediment remains similar than below, but sulphide banding reappears gradually. Sulphide bands grow thicker upcore and have a varved behaviour until 4.8 m depth, after which the banding fades away. Grain size has an increasing trend in the unit while organic content and magnetic susceptibility decrease, it's oscillatory behaviour becoming more irregular. These are interpreted as *Littorina* Sea phase sediments deposited in shallowed water depth. From 4 m upward the grain size increases and the silty sulphide sediment transitions to dark grey coarse silt with sandy sections and a few sulphide bands at 3 m depth in the sub-unit KY15-U5B (3–0.5 m). This is interpreted as beach deposits with redeposition and sandy layers originating from storm events in the shallowing bay during the final uplift from the sea. The remixing is supported by radiocarbon date signalling a mix of older redeposited material and sediment deposited during this time. The top 1 m features sand with some coarser ~1 cm layers with a sharp contact to fine detritus gyttja representing

final isolation from the sea. The isolation time is dated from fine detritus gyttja at 0.61 m depth to ~4300 cal BP.

To conclude, the unit U1 represents a highly dynamic postglacial sedimentation setting with low organic content and coarser, variable grain size, reflected in the magnetic susceptibility pattern. The unit U2 represents lacustrine *Ancylus* sediments as grey uniform silts with stable magnetic susceptibility and grain size with occasional coarse layers. Unit U3 corresponds to the *Littorina* transition with increasing organic content, magnetic susceptibility, and sulphide banding. Unit U4 features dark greenish grey to black sulphide sediments deposited during the *Littorina* Sea phase. The unit U5 with beach deposits feature lower organic content, coarser grain size and a marked change in the sedimentation during approaching isolation.

## Environmental magnetism

Environmental magnetic results are presented in Table 3 and Figs. 2 and 3. Due to the more dynamic sedimentation environments of the units U1 and U5, where differences in sediment characteristics are mainly driven by changes in melt-water quantities during deglaciation (U1) and near-shore mixing during shallowing into a beach environment (U5), the magnetic properties are

suspected to be driven by changes in the grain size and organic content. In units U2–U4 where lithological features remain relatively similar, magnetic susceptibility is suggested to be driven by changes in the magnetic mineralogy. Therefore, environmental magnetic methods were applied for discrete subsamples from units U2, U3 and U4, while units U1 and U5 were not further studied.

To study magnetic mineralogy more detailed, thermomagnetic analyses were applied for the subsamples from U2–U4 (Fig. 3). Subsamples from all units show a low temperature Verwey transition at ca  $-150^{\circ}\text{C}$  (Fig. 3a) suggesting that the subsamples contain stoichiometric magnetite (Dunlop and Özdemir 1997). Heating subsamples from room temperature to  $700^{\circ}\text{C}$  shows clearly distinct behaviour between different units indicating different magnetic mineral assemblages (Fig. 3b–d). Subsamples from all units show irreversible behaviour during heating and cooling cycles indicating thermal alteration of the initial magnetic minerals (Fig. 3b–d).

### Environmental magnetic characteristics of unit U2 Ancylus lake sediments

The greenish grey, at times faintly mottled Ancylus lake silts have even, low organic content, and grain size apart from occasional sandy layers. Concentration of magnetic minerals in the lacustrine silts is low, with lowest and very uniform magnetic susceptibility and SIRM values among the studied units ( $0.5\text{--}0.6 \times 10^{-6} \text{ m}^2 \text{ kg}^{-1}$  and  $1.8\text{--}3.7 \text{ Am}^2 \text{ kg}^{-1}$ , respectively) (Fig. 2). A relatively high S-ratio ( $-0.8\text{--}0.7$ ) suggests the magnetic minerals to be predominantly ferrimagnetic. Similarly, coercivity of natural remanent magnetization ( $\text{NRM}_{\text{MDF}}$ ) and

Bg values are low and uniform compared to the upper units. According to  $\text{NRM}_{\text{MDF}}$  ( $23\text{--}29 \text{ mT}$ ) and close to zero RRM ( $-0.6\text{--}0.9 \times 10^{-6} \text{ Am}^2 \text{ kg}^{-1}$ ) values, the Ancylus silts contain purely magnetite. Comparably low susceptibility of ARM ( $\chi_{\text{ARM}}$ ,  $0.5\text{--}0.9 \times 10^{-6} \text{ m}^3 \text{ kg}^{-1}$ ) coupled to high  $\chi_{\text{ARM}}/\text{SIRM}$  ( $24\text{--}28 \times 10^{-6} \text{ mA}^{-1}$ ) indicates that magnetic grains are predominantly in SD-size range (Maher 1988), but their total amount is low compared to other units. These findings are supported by the close to zero Bg ( $-1.1\text{--}1.6 \mu\text{T}$ ) corresponding to SD magnetite (Snowball 1997b, Hounslow *et al.* 2023). Four subsamples in the lower part of the unit acquired a positive frequency dependent susceptibility ( $\chi_{\text{fd}} = 3.1\text{--}4.6\%$ ), indicating the presence of small  $< 0.05 \mu\text{m}$  SD to SP size grains in the subsamples (Dearing *et al.* 1996), while subsamples from above 27 m depth did not show the presence of SP grains. In thermomagnetic measurements, subsamples from unit U2 show a wide, but prominent Hopkinson peak around  $470^{\circ}\text{C}$ , which decays by  $562^{\circ}\text{C}$  (Fig. 3b). This peak is associated with the newly formed magnetite with a wide range of grain sizes (Muxworthy *et al.* 2002) from oxidation of different iron bearing minerals present in the sediments of U2 and conversion into magnetite. In addition, a second decay at  $\sim 580^{\circ}\text{C}$  is obtained, indicating the presence of stoichiometric magnetite. During cooling to room temperature there is an increase in the magnetic susceptibility and throughout cooling  $\chi$  remains higher than during heating.

### Environmental magnetic characteristics of unit U3 Transition to Littorina Sea

With the transitioning to the marine Littorina Sea phase sulphide banding appears. The silty

**Table 3.** Values of environmental magnetic properties measured from discrete subsamples and mean magnetic susceptibility surface scan results.

Depth m	Unit	n	$\kappa$ $10^{-3}$ SI	$\chi$ $10^{-6}$ $\text{m}^3 \text{ kg}^{-1}$	SIRM $10^{-3}$ $\text{A m}^2 \text{ kg}^{-1}$	S-ratio	$\text{NRM}_{\text{MDF}}$ mT	RRM $10^{-6}$ $\text{A m}^2 \text{ kg}^{-1}$	Bg mT	$\chi_{\text{ARM}}$ $10^{-6}$ $\text{m}^3 \text{ kg}^{-1}$	$\chi_{\text{ARM}}/\text{SIRM}$ $10^{-6}$ $\text{mA}^{-1}$	$\chi_{\text{fd}}^1$ % n
7–8	U4	3	0.58 (0.13)	1.0 (0.3)	12.5 (9.4)	-0.74 (0.02)	28.1 (5.4)	-38.2 (37.8)	-21.6 (15.2)	1.7 (0.8)	16.9 (4.6)	4.0 1
15–16	U4 lower	10	0.48 (0.16)	1.2 (0.6)	42.5 (25.5)	-0.74 (0.07)	44.3 (3.3)	-283.2* (272.5)	-57.3 (15.7)	5.4 (4.5)	12.8 (3.4)	2.6 2
19–21	U3	4	0.49 (0.12)	1.0 (0.1)	31.5 (13.3)	-0.61 (0.03)	45.7 (2.8)	-153.0 (70.3)	-58.6 (11.3)	3.1 (1.1)	10.4 (1.4)	2.2 1
21–33	U2	6	0.35 (0.08)	0.6 (0.1)	2.9 (0.7)	-0.74 (0.03)	27.2 (1.9)	-0.8 (0.1)	-1.4 (0.1)	0.7 (0.1)	25.6 (1.3)	3.9 4

Mean (standard deviation)

$\kappa$  values from only the depths where environmental magnetic subsamples are collected.

<sup>1</sup> average results calculated only from subsamples that reached  $> 0.5\%$   $\chi_{\text{fd}}$  values.

n refers to the number of subsamples that the mean is calculated from.

\* One subsample (15.45 m) excluded from result

sediments have a uniform grain size and an increasing trend in both organic content and magnetic susceptibility. Magnetic susceptibility increases and oscillates with a growing range (Fig. 2). Concentration of magnetic minerals is growing, indicated by the magnetic susceptibility and SIRM values considerably higher than in Ancylus lake sediments ( $0.9\text{--}1.1 \times 10^{-6} \text{ m}^2 \text{ kg}^{-1}$  and  $13\text{--}42 \text{ Am}^2 \text{ kg}^{-1}$  respectively). In this unit, S-ratio ( $-0.65\text{--}0.57$ ) indicates a weak contribution from detrital hematite, but also here ferrimagnetic minerals are the main carriers of the magnetic signal. A change in magnetic mineralogy from Ancylus lake sediments is indicated with an increased  $\text{NRM}_{\text{MDF}}$  ( $42\text{--}48 \text{ mT}$ ). Also, RRM, Bg and  $\chi_{\text{ARM}}$  increase between U2 and U3 (measurement depths 19.9 m and 20.9 m respectively) with orders of magnitude greater values in U3 (Table 3). High negative RRM ( $-54\text{--}213 \times 10^{-6} \text{ Am}^2 \text{ kg}^{-1}$ ) and Bg ( $-43\text{--}70 \text{ } \mu\text{T}$ ) with the  $\text{NRM}_{\text{MDF}}$  indicate presence of greigite (Snowball 1997b). Furthermore, low  $\chi_{\text{ARM}}/\text{SIRM}$  ( $9\text{--}12 \times 10^{-6} \text{ mA}^{-1}$ ) together with the high negative RRM and Bg values are characteristic for diagenetic SD-greigite (Snowball 1997b). One subsample has signs of minor contribution of SP grains at  $2.2\% \chi_{\text{fd}}$ . During thermomagnetic analyses, subsamples feature a slight increase in magnetic susceptibility in the warming curve followed by a decrease of  $\chi$  between  $\sim 360\text{--}460^\circ\text{C}$ , interpreted to be associated with the thermal decomposition greigite (Krs *et al.* 1992, Roberts 1995, Dekkers *et al.* 2000, Muxworthy *et al.* 2023) (Fig. 3c). This is followed with a minor peak that decays at  $580^\circ\text{C}$  for one subsample and at  $600^\circ\text{C}$  for the two others, associated to original stoichiometric magnetite and possibly maghemite. The cooling curves have a slightly higher  $\chi$  than heating curves, but no prominent peaks are obtained.

#### Environmental magnetic characteristics of unit U4 Littorina Sea sulphide laminated sediments

The strongly laminated very dark sulphide silt deposited during the Littorina Sea phase has an even grain size but a highly variable oscillating magnetic susceptibility and slightly elevated

organic content. Magnetic enhancement is most pronounced in these sediments, as magnetic susceptibility and SIRM are highest of the studied units ( $0.6\text{--}2.6 \times 10^{-6} \text{ m}^2 \text{ kg}^{-1}$  and  $4\text{--}95 \text{ Am}^2 \text{ kg}^{-1}$  respectively), indicating a high concentration of ferrimagnetic minerals. S-ratio is in a similar but wider range as in Ancylus sediments ( $-0.9\text{--}0.6$ ), indicating that magnetic mineralogy consists of predominantly ferrimagnetic minerals and in some subsamples maybe also hematite. Most parameters have the largest variation in Littorina Sea sediments, values and variation decreasing again up-core. RRM and Bg have highest negative values of the studied units that decrease up-core (U4 lower:  $-11\text{--}991 \times 10^{-6} \text{ Am}^2 \text{ kg}^{-1}$  and  $-19\text{--}73.0 \text{ mT}$ ; U4 upper:  $-3\text{--}90 \times 10^{-6} \text{ Am}^2 \text{ kg}^{-1}$  and  $-4\text{--}41 \text{ mT}$ ). Based on these, magnetic enhancement is mainly driven by SD-greigite as pictured in U3, but the mineral assemblage / characteristics alter within the unit. Magnetic mineralogy is dominated by greigite in the lower Littorina Sea sediments as in Littorina transition. In the upper part of the unit ( $7\text{--}8 \text{ m}$  depth), most parameters decrease to or below the levels of U3. E.g., the  $\text{NRM}_{\text{MDF}}$  decreases and values are more variable ( $23\text{--}35 \text{ mT}$ ) indicating possibly less greigite and more magnetite. Magnetic grain size is similar than in sediments below, while three subsamples also have indications of SP-grains ( $\chi_{\text{fd}}$   $1.7\text{--}4.0 \%$ ). The thermomagnetic behaviour of the subsamples varies between upper and lower unit (Fig. 3d). A similar hump followed by decay between  $\sim 340\text{--}460^\circ\text{C}$  is obtained during heating as in U3 interpreted to indicate thermal decomposition of greigite. This feature is more prominent in subsamples in the lower part of the unit. A second decay occurs at  $580^\circ\text{C}$  or  $600^\circ\text{C}$  corresponding to the presence of stoichiometric magnetite and possibly maghemite. In some cases, a Hopkinson-like peak around  $500\text{--}550^\circ\text{C}$  precedes the decay, marking newly formed magnetite. Magnetic susceptibility increases upon cooling for most U4 subsamples due to new magnetite formed. Some cooling curves feature a Hopkinson peak at  $\sim 320$  to  $340^\circ\text{C}$ , indicating pyrrhotite formation from pyrite during heating (Wang *et al.* 2008). Since this was not prominent for all subsamples, probably only a small amount of pyrite is present in these Littorina sulphide sediments.

To conclude, magnetic susceptibility fluctuations are driven by either lithological features where grain size and organic content fluctuate (U1, U5) or magnetic mineral composition changes (U2, U3, U4) in units with fairly stable organic content and grain size. According to remanent magnetizations and temperature dependent magnetic susceptibility, the magnetic signal of laminated sulphide sediments (U3–U4) is produced by both SD greigite and magnetite, while freshwater silts (U2) contain purely SD magnetite.

## Discussion

### Sedimentary environment

The ~40-meter sediment record is estimated to represent ca 6.3 ka period from local deglaciation to uplift during the HTM, giving a mean average annual sedimentation rate of 0.65 cm. Typically Holocene marine and lacustrine sedimentary records surrounding the Baltic Sea are less than 10 m in length. The sediment record is dated with four radiocarbon dates, one from bulk sediment organic matter from unit U5A and three others from macrofossils from unit U4. The age-depth model used in this study should only be considered suggestive due to limited dating results, and thus sedimentation rates or temporal resolution will not be discussed further.

The deglaciation dynamics in the lateral margin of two ice masses have been multiphased and unordinary (Putkinen *et al.* 2020, Malinowski *et al.* 2023). The retreating ice sheet configuration was favourable to prevent the ancient bedrock valley in the study site vicinity (Hall *et al.* 2021) from filling with the thick coarse marginal deglaciation deposits typical for Kurikka region and allowed for an unremarkably long sequence of Baltic Sea sediments to deposit in the bedrock depression. The study site is neighbored by an extensive interlobate esker system (Niemelä *et al.* 1993) that deglaciated between 10 500–10 600 years ago (Stroeven *et al.* 2016). The base of KY15 sediment record (U1) is interpreted to feature flank sands from this esker, continuing as a high-energy basin sedimentation where the laminated sandy deposits are interlain

with fines deposited from suspension. With proceeding deglaciation and undulating ice streams lateral marginal position, the sediment input and the quantity of meltwater have probably fluctuated, leading to varied lamination thickness. Similar sediments have been described in the Baltic Sea region as glacial/sandy outwash (e.g., Virtasalo *et al.* 2007, Hyttinen *et al.* 2017, Jensen *et al.* 2017).

Sediments above the sandy outwash in the top part of unit U1 consist of glaciolacustrine rhythmites, typical for Baltic Sea sediments (Winterhalter 1992, Virtasalo *et al.* 2007, Andrén *et al.* 2014, Hyttinen *et al.* 2017). The fining of grain size indicates sedimentation in a deeper basin where the ice margin has receded from the vicinity. The glaciolacustrine rhythmite transitions within a short section (~10 cm) into homogenous silt in unit U2. The lithology of the sediment in this unit corresponds chiefly to descriptions of homogenous postglacial clay deposited during the Ancylus lake phase (Winterhalter 1992, Virtasalo *et al.* 2007, Andrén *et al.* 2014). During this time, barren land areas sensitive to erosion became exposed from under Baltic Ice Lake and were deposited in the Baltic Sea basin. Hence, the lacustrine phase was oligotrophic with a low organic production, causing low organic contents in the depositing sediments (Sohlenius *et al.* 1996, Andrén *et al.* 2011). In the Kurikka sediment record, sulphide banding is not observed within Ancylus lake sediments. Instead, the sediments feature increasing mottling upcore in this unit.

The gradually increasing organic content and magnetic susceptibility as well as the transition of postglacial lacustrine silts to sulphide banded sediment in the unit U3 indicate the transition to a marine phase (Andrén *et al.* 2011). The sulphide sediments in unit U3 and U4 correspond to the description of brackish water mud deposited during Littorina Sea phase (Winterhalter 1992, Andrén *et al.* 2000b, Zillén *et al.* 2008, Virtasalo *et al.* 2016, Hyttinen *et al.* 2017). According to Virtasalo *et al.* (2016), the base of the brackish water mud can be used as a regional stratigraphic marker across the Baltic Sea basin. Here, this contact is found at the base of U3, where the colour and structure of sediment changes notably from light grey mottled silt to clearly sulphide

banded / laminated silt with a slightly elevated organic content. However, no erosional surface or sandy layer marking marine flooding was seen. Moreover, since no biostratigraphical or dating control is available, the onset of Littorina transition cannot be precisely identified. Sediment in these units is mostly laminated sulphide gyttja silt, but at times sediment is very dark black and rather homogenous. The absence of laminae is thought to indicate increased bioturbation and thus more oxic bottom conditions in the otherwise hypoxic Littorina Sea environment (Zillén *et al.* 2008). The occasional white lines could be bacterial growth produced in hypoxic conditions by *Beggiatoa*, or alternatively, diatom layers. The increase in organic content indicates increased production, but the organic content in the studied sediment record is notably lower than in similar offshore deposits, where total organic carbon regularly exceeds 10 wt% (Moros *et al.* 2020). The salinity of the Baltic Sea basin increased as a consequence of relative sea level rise (Andrén *et al.* 2011), leading to extensive hypoxia across the basin (Zillén *et al.* 2008). Occasional coarser grained bands that become more common upcore in the unit suggest disruptions in the otherwise very peaceful bay setting. Sandy bands could indicate either intensifying near-shore influence in the shallowing basin or sporadic increase in clastic input from terrestrial sources.

In the unit U5A, the decrease in magnetic susceptibility and organic content and the sulphide bands become fewer and rhythmic in nature, which indicate the system changing into a mode where more frequent coastal processes maybe together with increased freshwater input control the bottom oxygen conditions. The shallowing is seen as the coarsening of grain size indicating a higher-energy system with increased wave action and more sediment being redeposited from the banks into the coastal basin. The rhythmic nature of laminae could result from e.g. spring flooding producing pulses of terrestrial matter on top of the dark fine winter laminae, phasing into a lamina with more organic content as the spring shifts to summer. There is a change in sedimentation at 3 m core depth (U5B), where magnetic susceptibility and organic content decrease, grain size coarsens, and sulphide

lamination disappears completely. Coarse silt indicates that waves and currents dominate the sedimentation environment. There are no clear sedimentary structures indicating that the material is reworked. The radiocarbon date from 0.91 m depth (Table 1) confirms, that the sediment contains a mixture of fresh and reworked older organic matter. Uplift to sea level and final isolation can be seen as repeated sandy gravel layers at 0.9–0.63 m depth followed by an erosional contact, where sandy sediment cuts into a thin layer of fine detritus gyttja deposited into a shallow pond. The radiocarbon date from the bottom of the fine detritus gyttja gives the minimum age for isolation at 4.3 ka cal BP.

### Environmental magnetic characteristics

According to the environmental magnetic results, there are three distinctive zones with different magnetic records in the studied units: 1) unit U2 Ancyclus lake sediments: amount of magnetic material is small, and the parameter values are constant; 2) U3 Littorina transition: amount of magnetic material increases; and 3) U4 Littorina Sea sulphide sediments: oscillatory magnetic enhancement. Median destructive field of natural remanent magnetization ( $\text{NRM}_{\text{MDF}}$  23–48 mT) and S-ratio (–0.89––0.57) indicate that ferrimagnetic minerals are present along the whole studied sediment sequence. Generally, the trends in mass magnetic susceptibility ( $\chi$ ), SIRM,  $\text{NRM}_{\text{MDF}}$ , rotational remanent magnetization (RRM), gyro field (Bg) and susceptibility of ARM ( $\chi_{\text{ARM}}$ ) from discrete subsamples correspond to magnetic susceptibility ( $\kappa$ ) trends throughout the units U2, U3 and U4, while mean S-ratio is relatively constant throughout these units. For these units  $\kappa$  varies in the range of 0.2– $0.8 \times 10^{-3}$  SI with maximum values and biggest variation obtained in the units U3 and U4. Similarly, SIRM values are lowest ( $3 \times 10^{-3} \text{ Am}^2 \text{ kg}^{-1}$ ) for the unit U2 and one order of magnitude higher for the units U3 and U4 ( $40\text{--}95 \times 10^{-3} \text{ Am}^2 \text{ kg}^{-1}$ ). The  $\text{NRM}_{\text{MDF}}$  is lowest (23–29 mT) in U2, and it increases in the U3–U4 to the highest of the sediment sequence (42–48 mT). In the upper part of the unit U4  $\text{NRM}_{\text{MDF}}$  decreases and is more vari-

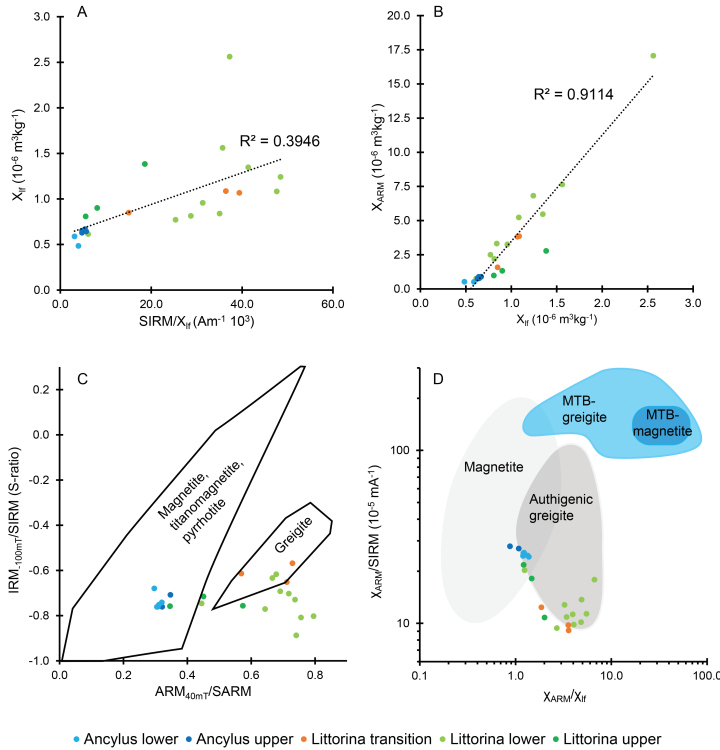


**Fig. 4.** Biplots for magnetic mineral characterization. **a)** Low-field magnetic susceptibility vs. SIRM/ magnetic susceptibility; **b)** Susceptibility of ARM vs. magnetic susceptibility; **c)** S-ratio vs.  $ARM_{40mT}/SARM$ . Ferrimagnetic mineral determination following Peters & Thompson (1998); **d)** Susceptibility of ARM/SIRM vs. Susceptibility of ARM/magnetic susceptibility. Categorization between different origins of greigite and magnetite, modified after Snowball (1994) and Reinholdsson *et al.* (2013).

able (23–35 mT). High (negative) RRM values follow high magnetic susceptibility ( $\kappa$ ) values and  $B_g$  behaves like RRM, but with a smaller range. The values of  $B_g$  vary from  $\sim -1.0$  mT in U2 up to  $-73.0$  mT for U3 and U4.  $\chi_{ARM}$  varies from  $0.5 \times 10^{-6}$  m<sup>3</sup>/kg for U2 to more than  $10 \times 10^{-6}$  m<sup>3</sup>/kg for U3 and U4. Range for S-ratio is from  $-0.89$  to  $-0.57$ , with the mean of  $-0.72$  (Table 3). The presence of greigite was studied with RRM, effective gyrofield ( $B_g$ ),  $NRM_{MDF}$  and thermomagnetic measurements. The thermomagnetic measurements support other environmental magnetic method results, with most subsamples in U4 and U3 showing decay of magnetic susceptibility around 360–460°C, interpreted to indicate thermal decomposition of SD-sized greigite. SD-sized magnetite is present at varying oxidation states in all units and subsamples. Pyrite is present in the middle U4 subsamples evidenced by pyrrhotite formation during heating (e.g. Wang *et al.* 2008, Muxworthy *et al.* 2023) and Energy Dispersive X-ray Spectroscopy (EDS) analysis (see details in Supplementary Information section S5 and Fig. S4).

### Greigite in the Bothnian coastal zone

Presence of greigite is indicated from various indicative ratios of magnetic parameters (Fig. 4) in addition to the negative values of RRM and effective gyrofield ( $B_g$ ),  $NRM_{MDF}$ , thermomagnetic measurements and EDS analysis (Fig. S4 in Supplementary Information).  $SIRM/\chi_{lf}$  values for Littorina transition and Littorina Sea phase (U3–U4) subsamples are high (22–50  $kAm^{-1}$ ) (Fig. 4a) being indicative for greigite (Roberts 1995, Dekkers and Schoonen 1996, Snowball 1997a, Sagnotti and Winkler 1999, Larrasoana *et al.* 2007, Roberts *et al.* 2011, Liu *et al.* 2012).  $\chi_{ARM}$  (Fig. 4b) values, which discriminate SD grain sizes, are high for these same subsamples, as are also the values for  $\chi_{ARM}/\chi_{lf}$  ratio (Fig. 4d), indicating high relative contribution of SD grains in U3–U4 (e.g., Banerjee *et al.* 1981, Evans and Heller 2003).

Biplots to distinguish different ferrimagnetic minerals and their origin are shown in Figs. 4c and 4d.  $IRM_{(-100mT)}/SIRM$  (S-ratio) versus  $ARM_{(40mT)}/SARM$  (i.e.  $ARM_{(0)}$ ) can be

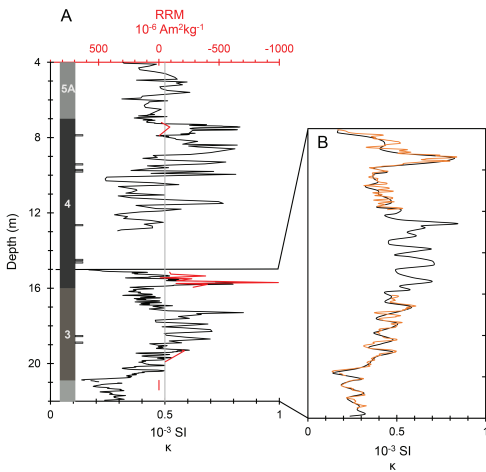


**Fig. 5. a)** Comparison of magnetic susceptibility (black; composite of 10 cm and 1 cm resolution records) and RRM (red) values. Coloured bar next to depth-axis indicates lithological units and their approximate appearance. Grey bars next to the lithological units mark thin coarser silty bands in the sediment. The grey vertical line shows the threshold magnetic susceptibility value for greigite occurrence. **b)** a comparison between 10 cm (black) and 1 cm (orange) interval magnetic susceptibility record is shown.

used to indicate different ferrimagnetic minerals as described by Peters and Thompson (1998).  $\chi_{\text{ARM}}/\text{SIRM}$  versus  $\chi_{\text{ARM}}/\chi_{\text{IF}}$  was used by Reinholdsson *et al.* (2013) to distinguish minerals formed authigenically from those formed through biomineralization by magnetotactic bacteria. S-ratio values ( $< -0.6$ ) (Fig. 4c) indicate the presence of ferrimagnetic minerals in all the studied subsamples. Furthermore, based on ferrimagnetic determination diagram (Peters and Thompson 1998) (Fig. 4c), the dominant ferrimagnetic mineral in Littorina transition and Littorina Sea phase subsamples is greigite, whereas the Ancyclus and upper Littorina Sea phase subsamples show lower  $\text{ARM}_{(40\text{mT})}/\text{SARM}$  values indicating non-bacterial SD magnetite. Further on, the subsamples fit to authigenic greigite threshold values characterized by Reinholdsson *et al.* (2013), where authigenic SD-greigite show lower  $\chi_{\text{ARM}}/\text{SIRM}$  values than greigite formed by magnetotactic bacteria (Fig. 4d). However, authigenic greigite could perhaps overprint a weak contribution of biogenic greigite and while the signature of authigenic greigite is clear, co-occurring population of biogenic greigite cannot be ruled out.

Figure 4a shows positive correlation between high magnetic susceptibility values and the presence of greigite in subsamples ( $r_{\text{pearson}} = 0.63$ ,  $p_{\text{two-tailed}} = 0.001$ ;  $r_{\text{spearman}} = 0.85$ ,  $p_{\text{two-tailed}} < 0.001$ ). The higher magnetic susceptibility values correlate also well to the SD-size range (Fig. 4b) ( $r_{\text{pearson}} = 0.96$ ,  $p_{\text{two-tailed}} < 0.001$ ;  $r_{\text{spearman}} = 0.94$ ,  $p_{\text{two-tailed}} < 0.001$ ). The findings suggest that high magnetic susceptibility along the sediment core in the studied units (U2–U4) indicates the presence of SD-greigite, and low magnetic susceptibility indicates magnetite. Naturally, with a limited amount and coverage of environmental magnetic subsamples, changes in magnetic carriers within these zones cannot be ruled out. However, magnetic susceptibility appears to echo the environmental magnetic characteristics of the sediment sequence, allowing the use of magnetic susceptibility record as a proxy for changing magnetic minerals and hence, assessment of changing bottom conditions during mineral formation. Based on the connection between magnetic susceptibility and (magnetic mineral indicative) environmental magnetic parameters (Fig. 4a, 4b), changes in magnetic susceptibility reflect the occurrence and concentration of greigite. In the interpretation of the sediment sequence, the threshold value of magnetic susceptibility for significant greigite occurrence in the Kurikka sediment sequence is estimated to  $0.5 \times 10^{-3}$  SI (Fig. 5). While most of the samples below this have RRM values close to zero, four greigite-containing depths exhibit magnetic susceptibility values between  $0.3$ – $0.5 \times 10^{-3}$  SI. Detailed studies would be needed to explain the slightly different signatures of the individual subsamples in this transitional zone, confirm the composition of magnetic assemblages throughout the sediment sequence, and to clarify the timing of the formation of various magnetic phases.

Greigite has been identified in Baltic Sea sediments several times (Sohlenius 1996, Leland and Stevens 1998, Berglund *et al.* 2005, Kortekaas 2007, Reinholdsson *et al.* 2013, Holmkvist *et al.* 2014), although many of these observations are not based on magnetic measurements. Authigenic greigite was identified in Yoldia Sea brackish water sediments (Sohlenius 1996), Ancyclus lake sediments (Lougheed *et al.* 2012, Reinholdsson *et al.* 2013), Littorina transition

sediments (Berglund *et al.* 2005) and Littorina Sea laminated sapropels (Sohlenius 1996, Leland and Stevens 1998). Most recently, through more detailed magnetic and Transmission Electron Microscope (TEM) measurements, Littorina Sea sapropels deposited in central Baltic deep basins were found to contain biomineralized SD-greigite most likely produced by magnetotactic bacteria (Reinholdsson *et al.* 2013), bringing the question of the origins of greigite in Baltic Sea sediments for consideration. The formation environment for the central Baltic sediments containing magnetosomal greigite has been previously proposed having long periods of continuous hypoxia and periodical euxinia during the HTM (Sohlenius *et al.* 2001, Zillén *et al.* 2008). The Kurikka record confirm multiple formation pathways for greigite growth in Baltic Sea sulphide sediments highlighting the different processes in Baltic deep basins compared to coastal zone. According to Häusler *et al.* (2017), the bottom conditions in central Bothnian Sea were — as opposed to the central Baltic Sea — probably long-term hypoxic but non-euxinic during local HTM based on the occurrence of Mn(Ca)CO<sub>3</sub> layers. In Kurikka, SD-greigite is observed without signs of pyrrhotite, indicating greigite formation in the sulphidic zone (Roberts *et al.* 2018). Further on, the thermomagnetic analyses indicated the presence of pyrite and absence of pyrrhotite in lower Littorina Sea sediments (Fig. 3), supporting formation in the sulphidic zone. In addition to the differences in water chemistry, coastal areas with shallower water depth have more pronounced mixing and hypoxia could be mainly seasonal (van Helmond *et al.* 2017). Hence, different formation environments (continuous hypoxia and periodical euxinia vs. (seasonal) hypoxia, no euxinia) might lead to different origins of greigite.

We suggest that in the coastal zone, the low organic content and high sedimentation rate during Littorina Sea phase support authigenic greigite production due to the ratio between reactive iron content and organic content favouring greigite formation (e.g., Kao *et al.* 2004, Rowan and Roberts 2006). Similarly, greigite might be preserved due to the relatively rapid accumulation rate arresting pyritization (Kao *et al.* 2004, Blanchet *et al.* 2009, Chen *et al.* 2021). In a near-shore sedimentary environment the accumulation

of terrestrial sediment into the shallowing bay has probably been considerably larger than that in the Baltic deep basins. Authigenic greigite formation in Kurikka shows that in an epicontinental basin like the Baltic Sea, greigite origin can vary across similar sediments, highlighting the key role of the sedimentary environment, from coastal to deep settings.

### Oxygen variability in the Bothnian Coastal zone during HTM

The correlation between magnetic susceptibility and the environmental magnetic characteristics of the sediment sequence (Fig. 4) allows the use of magnetic susceptibility record as a proxy for changing bottom conditions during mineral formation. While greigite can be formed also after deposition at any time during diagenesis, the rapid burial likely limited postdepositional alteration and could enable both greigite and magnetite preservation. Moreover, the varying mineralogy and magnetic susceptibility indicate changing conditions in the system. Hence, the threshold value for significant greigite occurrence ( $0.5 \times 10^{-3}$  SI, Fig. 5) is considered also a threshold for deoxygenation, and changes in oxygen conditions are assessed based on the magnetic susceptibility record. The ability of the 10 cm interval magnetic susceptibility record to depict fine-scale changes was evaluated by comparing it with 1 cm interval magnetic susceptibility in four parts of the sediment sequence (Fig. 5). The 10 cm magnetic susceptibility traces generally very well fine-scaled cyclicity, allowing the detailed use of the 10 cm magnetic susceptibility record throughout the whole sediment sequence. At only 16–17 m depth, the oscillation was found to be more fine-scaled than what was depicted by the 10 cm magnetic susceptibility record.

### Kurikka deoxygenation history based on the magnetic susceptibility record

Based on the Kurikka magnetic susceptibility record and mean assumed sedimentation rates, deoxygenation in the Kurikka bay has been common during HTM from Littorina transition

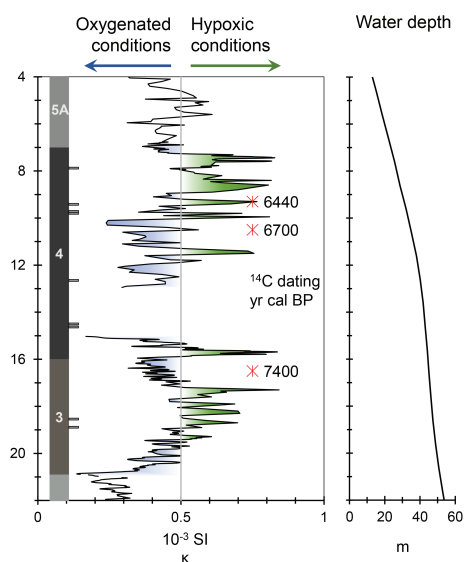


**Fig. 6.** Interpretation on oxygen deficiency derived from the magnetic susceptibility record. Green indicates increasing oxygen deficiency (hypoxia) while blue indicates oxic conditions. Red asterisks mark radiocarbon dates, shown as years cal BP. Coloured bar on left indicates lithological units and coarser sandy bands in sediment are marked with small horizontal bars next to the unit bar. Water depth as inferred from the relative shoreline displacement curve and tentative age-depth model of sediment record.

to Littorina Sea phase ca 8–6 ka cal BP years ago (interval at 7–20 m depth), but not continuous (Fig. 6). Within this HTM interval, two multicentennial (~8–7.5 ka cal BP; 19–17 m depth and ~6.5–6 ka cal BP; 10–7 m) predominantly hypoxic periods and two intensive decadal (16–15 m and 12–11 m depth) hypoxic events are obtained. Between multicentennial hypoxic periods, a period with predominantly oxic conditions (17–15 and 13–10 m depth) is obtained. The predominantly oxic conditions are interrupted by at least two decadal hypoxic events around ~7 ka cal BP, but the total length and character of this period remains unknown because of a data gap in the magnetic susceptibility record (15–13 m). Within these multicentennial periods, concentration of magnetic minerals fluctuates. This could derive from changing / unstable bottom conditions. Greigite concentration in the sediment is highest during the older decadal event around 7 ka cal BP (16–15 m), indicating the maximum intensity of oxygen

depletion. Perennial variability in magnetic susceptibility is large between 12–7 m, coinciding with the shallowing of the water column from approximately 38 to 23 m depth. Above this, the termination of oxygen deficiency in the Kurikka sediment sequence is synchronous to lithological changes from marine to coastal high-energy sedimentation deriving from shallowing of the sedimentary system and the ultimate uplift above sea level. At times, lower magnetic susceptibility corresponds to the coarser silty bands seen in sediment (Fig. 6). A coarser layer could indicate for example a rise in relative sea level, redeposited beach sediments caused by increased bottom currents or wave action or a pulse of increased terrestrial input due to increased rainfall and erosion. All these scenarios would also explain a short weakening of hypoxia due to mixing of the water column.

### Comparison with Bothnian sea hypoxia records

The initiation of hypoxia in Kurikka around ~8 ka cal BP coincides with the start of the HTM hypoxic interval observed across the Baltic Sea (in central Bothnian Sea, ~7.8–7 ka (Jilbert *et al.* 2015, Häusler *et al.* 2017), in central Baltic Sea ~8–7.2 ka (Sohlenius *et al.* 2001, Zillén *et al.* 2008, Jilbert and Slomp 2013)). The HTM hypoxic interval is linked to the ingress of saline water into Baltic Sea ~8–7 ka, observed from the Danish Straits (e.g., Bennike *et al.* 2021) all the way to the Bothnian Sea (Häusler *et al.* 2017). A strong deep-water exchange from central Baltic to the Bothnian Sea was suggested due to a significantly deeper position of the sill between the basins from 8 until at least 4 ka (Jilbert *et al.* 2015). The coevality of the hypoxic interval across the Baltic Sea basin indicates that the effects of saline water intrusion were rapidly seen even in northern Baltic coastal systems. The rapid shift from freshwater to brackish conditions was also observed in the western coast of Bothnian Sea by Warnock *et al.* (2018). In the coast of the central Baltic Sea, hypoxia during HTM was found persistent (Ning *et al.* 2016), shifting to seasonal hypoxia with shallowing water depth from ~55 to 30 m after the HTM.

In the southern Baltic coast, hypoxia was found seasonal throughout the Holocene since the transition to Littorina Sea phase ~8 ka ago (van Helmond *et al.* 2017).

### Zonation & periodicity of hypoxia in Kurikka

The patterns of the hypoxic interval in Kurikka fit the description of the ~200–500-year multicentennial hypoxic events varying with intensity in the central Baltic Sea observed by Jilbert and Slomp (2013). The two multicentennial periods of more prevalent hypoxia and the predominantly oxic period in between in the Kurikka record fit well the description of a multicentennial nature of hypoxia variability. This periodicity of hypoxia in the Baltic Sea basin has been proposed to be forced by climate variability. The rapid intensification and termination of the hypoxic events are suggested to be driven by the feedbacks in the phosphorous cycle (Jilbert and Slomp 2013). The feedbacks in coupled iron– and phosphorous cycles have been thought to drive also smaller-scale changes in hypoxia intensity within the hypoxic events (Jilbert *et al.* 2021). While the oscillatory behaviour of hypoxia is evident in the Kurikka record, further investigations will allow for a more detailed look into the behaviour of hypoxia on short time scales. It has been suggested that eutrophication in the coastal environment is currently affected more by local terrestrial inputs and sea-ice cover duration, rather than large scale climatic or hydrospheric drivers responsible for deep basin eutrophication (Vigouroux *et al.* 2021). However, the similar patterns in Holocene oxygen condition variability in Kurikka and offshore records might suggest basin-wide regularity and drivers of hypoxia during HTM.

### Conclusions

The ~40 m sedimentary record from Kurikka represents the Holocene development of the shallowing northern Baltic Sea from the local deglaciation through the last Baltic Sea phases until local isolation from the Littorina Sea. The depositional environment transforms from offshore, ~190 m

water depth setting during Ancyclus lake phase to sheltered coastal Littorina sea conditions with 18 meters of sulphide sediment deposited. No sign of Littorina transgression is observed. The sediment record is topped with < 3 m of sandy beach deposits.

For Kurikka sediment sequence, the magnetic component of Ancyclus lake deposits (U2) was identified as magnetite only. Whereas in Littorina Sea deposits (U3–U4) both greigite and magnetite were detected by magnetic parameters. Results differ from central Baltic Sea Basin where both magnetite and greigite were present in Ancyclus sediments and only greigite was found in Littorina sediments.

Greigite in Littorina Sea deposits has magnetic properties characteristic of authigenic greigite, rather than magnetosomal greigite that has been found in the central Baltic Sea. In the coastal zone with substantial terrestrial input, the low organic content and high sedimentation rate during Littorina Sea phase might support authigenic greigite production due to the ratio between reactive iron content and organic content favouring authigenic greigite formation.

Hence, the Kurikka record confirm multiple formation pathways for greigite growth in Baltic Sea sediments highlighting the different processes in Baltic deep basins compared to coastal zone. The authigenic greigite origin in Kurikka indicates that the local sedimentation environment strongly governs greigite formation and its preservation even within same basin-wide stratigraphic units.

The correlation between high magnetic susceptibility and greigite occurrence (and perhaps quantity) allows the detailed magnetic susceptibility record to be used within the studied units as a proxy for greigite occurrence and hence, a proxy for past deoxygenation.

Based on this proxy, deoxygenation has been common but not continuous during the Littorina Sea phase. The initiation of deoxygenation coincides with the start of the HTM hypoxic interval observed across the Baltic Sea, indicating that the effects of saline water intrusion from Danish Straits were rapidly spread up to northern coastal systems. The pattern of oxygen conditions in Kurikka coastal setting corresponds to the multicentennial nature of hypoxia variability with oscillating intensity in the central Baltic Sea.

*Acknowledgements:* We thank the editor Niina Kuosmanen and reviewers Ian Snowball and anonymous for comments that greatly improved the manuscript. We are grateful for Lakshika Palamakumbure and Satu Vuoriainen for thermomagnetic analysis at GTK and the HelLabs staff for help with laboratory analysis, including Katie Doigh for the Microprobe operation.

*Funding:* This work was a cooperation between the University of Helsinki and the Geological Survey of Finland. It was supported by the Doctoral School of the University of Helsinki, Kurikka city, the municipal waterworks of Kurikka and Vaasa and HelLabs (UH).

This is number 26 of HelLabs publications.

*Supplementary Information:* The supplementary information related to this article is available online at: <http://www.borenav.net/BER/archive/pdfs/ber30/ber30-055-076-supplement.pdf>

## References

- Andrén E., Andrén T. & Kunzendorf H. 2000a. Holocene history of the Baltic Sea as a background for assessing records of human impact in the sediments of the Gotland Basin. *The Holocene* 10: 687-702.
- Andrén E., Andrén T. & Sohlenius G. 2000b. The Holocene history of the southwestern Baltic Sea as reflected in a sediment core from the Bornholm Basin. *Boreas* 29: 233-250.
- Andrén T., Björck S., Andrén E., Conley D.J., Zillén L. & Anjar J. 2011. The development of the Baltic Sea Basin during the last 130 ka. In: *The Baltic Sea Basin*, Springer, pp. 75-97.
- Andrén T., Andrén E. & Zhang R. 2014. *Baltic Sea Basin Paleoenvironment: paleoenvironmental evolution of the Baltic Sea Basin through the last glacial cycle*. Integrated Ocean Drilling Program.
- Banerjee S.K., King J. & Marvin J. 1981. A rapid method for magnetic granulometry with applications to environmental studies. *Geophysical Research Letters* 8: 333-336.
- Bennike O., Jensen J.B., Norgaard-Pedersen N., Andresen K.J., Seidenkrantz M.S., Moros M. & Wagner B. 2021. When were the straits between the Baltic Sea and the Kattegat inundated by the sea during the Holocene? *Boreas* 50: 1079-1094.
- Berglund B.E., Sandgren P., Barnekow L., Hannon G., Jiang H., Skog G. & Yu S.-Y. 2005. Early Holocene history of the Baltic Sea, as reflected in coastal sediments in Blekinge, southeastern Sweden. *Quaternary International* 130: 111-139.
- Blanchet C.L., Thouveny N. & Vidal L. 2009. Formation and preservation of greigite (Fe<sub>3</sub>S<sub>4</sub>) in sediments from the Santa Barbara Basin: Implications for paleoenvironmental changes during the past 35 ka. *Paleoceanography* 24.
- Boulton G.S., Dongelmans P., Punkari M. & Broadgate M. 2001. Palaeoglaciology of an ice sheet through a glacial cycle: the European ice sheet through the Weichselian. *Quaternary Science Reviews* 20: 591-625.
- Breitburg D., Levin L.A., Oschlies A., Grégoire M., Chavez F.P., Conley D.J., Garçon V., Gilbert D., Gutiérrez D. & Isensee K. 2018. Declining oxygen in the global ocean and coastal waters. *Science* 359: eaam7240.
- Bronk-Ramsey C. 2009. Bayesian analysis of radiocarbon dates. *Radiocarbon* 51: 337-360.
- Chen Y., Zhang W., Nian X., Sun Q., Ge C., Hutchinson S.M., Cheng Q., Wang F., Chen J. & Zhao X. 2021. Greigite as an indicator for salinity and sedimentation rate change: Evidence from the Yangtze River Delta, China. *Journal of Geophysical Research: Solid Earth* 126: e2020JB021085.
- Conley D.J., Björck S., Bonsdorff E., Carstensen J., Destouni G., Gustafsson B.G., Hietanen S., Kortekaas M., Kuosa H., Meier H.E.M., Müller-Karulis B., Nordberg K., Norkko A., Nurnberg G., Pitkanen H., Rabalais N.N., Rosenberg R., Savchuk O.P., Slomp C.P., Voss M., Wulff F. & Zillén L. 2009. Hypoxia-Related Processes in the Baltic Sea. *Environmental Science & Technology* 43: 3412-3420.
- Conley D.J., Carstensen J., Aigars J., Axe P., Bonsdorff E., Eremina T., Haahti B.-M., Humborg C., Jonsson P., Kotta J., Lännegren C., Larsson U., Maximov A., Medina M.R., Lysiak-Pastuszak E., Remeikaitė-Nikiėnė N., Walve J., Wilhelms S. & Zillén L. 2011. Hypoxia is increasing in the Coastal Zone of the Baltic Sea. *Environmental Science & Technology* 45: 6777-6783.
- De Vries H.L. & Barendsen G.W. 1954. Measurements of age by the carbon-14 technique. *Nature* 174: 1138-1141.
- Dean W.E. 1974. Determination of carbonate and organic matter in calcareous sediments and sedimentary rocks by loss on ignition; comparison with other methods. *Journal of Sedimentary Research* 44: 242-248.
- Dearing J.A., Dann R.J.L., Hay K., Lees J.A., Loveland P.J., Maher B.A. & O'Grady K. 1996. Frequency-dependent susceptibility measurements of environmental materials. *Geophysical Journal International* 124: 228-240.
- Dekkers M.J. & Schoonen M.A.A. 1996. Magnetic properties of hydrothermally synthesized greigite (Fe<sub>3</sub>S<sub>4</sub>)—I. Rock magnetic parameters at room temperature. *Geophysical Journal International* 126: 360+.
- Dekkers M.J., Passier H.F. & Schoonen M.A.A. 2000. Magnetic properties of hydrothermally synthesized greigite (Fe<sub>3</sub>S<sub>4</sub>)—II. High- and low-temperature characteristics. *Geophysical Journal International* 141: 809-819.
- Diaz R.J. & Rosenberg R. 2008. Spreading dead zones and consequences for marine ecosystems. *Science* 321: 926-929.
- Dijkstra N., Quintana Krupinski N.B., Yamane M., Obrochta S.P., Miyairi Y., Yokoyama Y. & Slomp C.P. 2018. Holocene Refreshening and Reoxygenation of a Bothnian Sea Estuary Led to Enhanced Phosphorus Burial. *Estuaries and Coasts* 41: 139-157.
- Dunlop D.J. & Özdemir Ö. 1997. *Rock magnetism: fundamentals and frontiers*. Cambridge University Press.
- Ebert Y., Shaar R., Levy E.J., Zhao X., Roberts A.P. & Stein M. 2020. Magnetic Properties of Late Holocene Dead Sea Sediments as a Monitor of Regional Hydroclimate.

- Geochemistry Geophysics Geosystems* 21: 15.
- Eronen M. 1974. *The history of the Litorina Sea and associated holocene events*. University of Helsinki, Helsinki.
- Evans M.E. & Heller F. 2003. *Environmental magnetism: principles and applications of enviromagnetics*. International Geophysics series, Academic press, Elsevier, California.
- Fennel K. & Testa J.M. 2019. Biogeochemical controls on coastal hypoxia. *Annual review of marine science* 11: 105-130.
- Froelich P.N., Klinkhammer G.P., Bender M.L., Luedtke N.A., Heath G.R., Cullen D., Dauphin P., Hammond D., Hartman B. & Maynard V. 1979. Early oxidation of organic matter in pelagic sediments of the eastern equatorial Atlantic: suboxic diagenesis. *Geochimica et Cosmochimica Acta* 43: 1075-1090.
- Fältmarsch R.M., Åström M.E. & Vuori K.-M. 2008. Environmental risks of metals mobilised from acid sulphate soils in Finland: a literature review.
- Gibbard P.L. & Lewin J. 2016. Filling the North Sea Basin: Cenozoic sediment sources and river styles (André Dumont medallist lecture 2014). *Geologica Belgica*.
- Glückert G., Rantala P. & Ristaniemi O. 1993. *Itämeren jääkauden jälkeinen rannansiirtyminen Pohjanmaalla*. Turun yliopiston maaperägeologian osaston julkaisuja, ISSN 0356-7400, Turun yliopisto, Turku.
- Gustafsson B.G. & Westman P. 2002. On the causes for salinity variations in the Baltic Sea during the last 8500 years. *Paleoceanography* 17: 12-11-12-14.
- Hall A.M., Putkinen N., Hietala S., Lindsberg E. & Holma M. 2021. Ultra-slow cratonic denudation in Finland since 1.5 Ga indicated by tiered unconformities and impact structures. *Precambrian Research* 352: 106000.
- Heiri O., Lotter A.F. & Lemcke G. 2001. Loss on ignition as a method for estimating organic and carbonate content in sediments: reproducibility and comparability of results. *Journal of Paleolimnology* 25: 101-110.
- Holmkvist L., Kamyshny Jr A., Bruechert V., Ferdelman T.G. & Jørgensen B.B. 2014. Sulfidization of lacustrine glacial clay upon Holocene marine transgression (Arkona Basin, Baltic Sea). *Geochimica et Cosmochimica Acta* 142: 75-94.
- Hounslow M.W., Horng C.-S. & Karloukovski V. 2023. Rotational remanent magnetization as a magnetic mineral diagnostic tool at low rotation rates. *Geophysical Journal International* 232: 300-321.
- Hyttinen O., Kotilainen A.T., Virtasalo J.J., Kekäläinen P., Snowball I.F., Obrochta S.P. & Andrén T. 2017. Holocene stratigraphy of the Ångermanälven river estuary, Bothnian Sea. *Geo-Marine Letters* 37: 273-288.
- Häusler K., Moros M., Wacker L., Hammerschmidt L., Dellwig O., Leipe T., Kotilainen A.T. & Arz H.W. 2017. Mid- to late Holocene environmental separation of the northern and central Baltic Sea basins in response to differential land uplift. *Boreas* 46: 111-128.
- Jensen J.B., Moros M., Endler R. & Members I.E. 2017. The Bornholm Basin, southern Scandinavia: a complex history from Late Cretaceous structural developments to recent sedimentation. *Boreas* 46: 3-17.
- Jilbert T. & Slomp C.P. 2013. Rapid high-amplitude variability in Baltic Sea hypoxia during the Holocene. *Geology* 41: 1183-1186.
- Jilbert T., Conley D.J., Gustafsson B.G., Funkey C.P. & Slomp C.P. 2015. Glacio-isostatic control on hypoxia in a high-latitude shelf basin. *Geology* 43: 427-430.
- Jilbert T., Gustafsson B.G., Veldhuijzen S., Reed D.C., van Helmond N.A.G.M., Hermans M. & Slomp C.P. 2021. Iron-Phosphorus Feedbacks Drive Multidecadal Oscillations in Baltic Sea Hypoxia. *Geophysical Research Letters* 48: e2021GL095908.
- Jokinen S.A., Virtasalo J.J., Jilbert T., Kaiser J., Dellwig O., Arz H.W., Hänninen J., Arppe L., Collander M. & Saarinen T. 2018. A 1500-year multiproxy record of coastal hypoxia from the northern Baltic Sea indicates unprecedented deoxygenation over the 20th century. *Biogeosciences* 15: 3975-4001.
- Kao S.-J., Horng C.-S., Roberts A.P. & Liu K.-K. 2004. Carbon-sulfur-iron relationships in sedimentary rocks from southwestern Taiwan: influence of geochemical environment on greigite and pyrrhotite formation. *Chemical Geology* 203: 153-168.
- Konert M. & Vandenbergh J.E.F. 1997. Comparison of laser grain size analysis with pipette and sieve analysis: a solution for the underestimation of the clay fraction. *Sedimentology* 44: 523-535.
- Kortekaas M. 2007. *Post-glacial history of sea-level and environmental change in the southern Baltic Sea*. Lund University, Department of Geology, Quaternary Sciences.
- Krs M., Novák F., Krsová M., Pruner P., Kouklíková L. & Jansa J. 1992. Magnetic properties and metastability of greigite-smythite mineralization in brown-coal basins of the Krušné hory Piedmont, Bohemia. *Physics of the Earth and Planetary Interiors* 70: 273-287.
- Larrasoña J.C., Roberts A.P., Musgrave R.J., Gràcia E., Piñero E., Vega M. & Martínez-Ruiz F. 2007. Diagenetic formation of greigite and pyrrhotite in gas hydrate marine sedimentary systems. *Earth and Planetary Science Letters* 261: 350-366.
- Lepland A. & Stevens R.L. 1998. Manganese authigenesis in the landsort deep, Baltic Sea. *Marine Geology* 151: 1-25.
- Li W., Mu G.J., Zhang W.G., Lin Y.C., Zhang D.L. & Song H.Z. 2019. Formation of greigite (Fe<sub>3</sub>S<sub>4</sub>) in the sediments of saline lake Lop Nur, northwest China, and its implications for paleo-environmental change during the last 8400 years. *Journal of Asian Earth Sciences* 174: 99-108.
- Liu Q., Roberts A.P., Larrasoña J.C., Banerjee S.K., Guyodo Y., Tauxe L. & Oldfield F. 2012. Environmental magnetism: principles and applications. *Reviews of Geophysics* 50.
- Lougheed B.C., Snowball I.F., Moros M., Kabel K., Muscheler R., Virtasalo J.J. & Wacker L. 2012. Using an independent geochronology based on palaeomagnetic secular variation (PSV) and atmospheric Pb deposition to date Baltic Sea sediments and infer 14C reservoir age. *Quaternary Science Reviews* 42: 43-58.
- Maher B.A. 1988. Magnetic properties of some synthetic sub-micron magnetites. *Geophysical Journal International*

- tional 94: 83-96.
- Malinowski M., Putkinen N., Brodic B., Laakso V., Koskela E., Heinonen S., Engström J. & Paananen M. 2023. P- and S-wave Seismic Imaging of a Complex Aquifer System in Kurikka, Western Finland. *First Break* 41: 67-72.
- Middelburg J.J. & Levin L.A. 2009. Coastal hypoxia and sediment biogeochemistry. *Biogeosciences* 6: 1273-1293.
- Moros M., Kotilainen A.T., Snowball I.F., Neumann T., Perner K., Meier H.E.M., Leipe T., Zillén L., Damste J.S.S. & Schneider R. 2020. Is 'deep-water formation' in the Baltic Sea a key to understanding seabed dynamics and ventilation changes over the past 7,000 years? *Quaternary International* 550: 55-65.
- Muxworthy A.R., Schmidbauer E. & Petersen N. 2002. Magnetic properties and Mössbauer spectra of urban atmospheric particulate matter: a case study from Munich, Germany. *Geophysical Journal International* 150: 558-570.
- Muxworthy A.R., Turney J.N., Qi L., Baker E.B., Perkins J.R. & Abdulkarim M.A. 2023. Interpreting high-temperature magnetic susceptibility data of natural systems. *Frontiers in Earth Science* 11: 1171200.
- Niemelä J., Ekman I. & Lukasov A. 1993. *Suomen ja Venäjän federaation luoteisosan maaperä ja sen raaka-ainevarat, 1:1 000 000*. Geologian tutkimuskeskus & Venäjän Tiedekatemia Karjalan Tiedekeskuksen Geologian instituutti.
- Ning W., Ghosh A., Jilbert T., Slomp C.P., Khan M., Nyberg J., Conley D.J. & Filipsson H.L. 2016. Evolving coastal character of a Baltic Sea inlet during the Holocene shoreline regression: impact on coastal zone hypoxia. *Journal of Paleolimnology* 55: 319-338.
- Peters C. & Thompson R. 1998. Magnetic identification of selected natural iron oxides and sulphides. *Journal of Magnetism and Magnetic Materials* 183: 365-374.
- Putkinen N., Ross M., Hall A.M. & Lindsberg E. 2020. A valley-fill sequence in old bedrock valleys provide evidence for complex cyclical interlobate and ice marginal fluctuations during the last deglaciation in west-central Finland. In: *Geological society of America virtual conference, October 26-30 2020*.
- Ramaswamy V. & Rao P.S. 2006. Grain size analysis of sediments from the northern Andaman Sea: comparison of laser diffraction and sieve-pipette techniques. *Journal of Coastal Research* 22: 1000-1009.
- Reimer P.J., Austin W.E.N., Bard E., Bayliss A., Blackwell P.G., Ramsey C.B., Butzin M., Cheng H., Edwards R.L. & Friedrich M. 2020. The IntCal20 Northern Hemisphere radiocarbon age calibration curve (0–55 cal kBP). *Radiocarbon* 62: 725-757.
- Reinholdsson M., Snowball I.F., Zillén L., Lenz C. & Conley D.J. 2013. Magnetic enhancement of Baltic Sea sapropels by greigite magnetofossils. *Earth and Planetary Science Letters* 366: 137-150.
- Roberts A.P. 1995. Magnetic properties of sedimentary greigite (Fe<sub>3</sub>S<sub>4</sub>). *Earth and Planetary Science Letters* 134: 227-236.
- Roberts A.P., Chang L., Rowan C.J., Hornig C.-S. & Florindo F. 2011. Magnetic properties of sedimentary greigite (Fe<sub>3</sub>S<sub>4</sub>): An update. *Reviews of Geophysics* 49.
- Roberts A.P., Zhao X., Harrison R.J., Heslop D., Muxworthy A.R., Rowan C.J., Larrasoña J.C. & Florindo F. 2018. Signatures of reductive magnetic mineral diagenesis from unmixing of first-order reversal curves. *Journal of Geophysical Research: Solid Earth* 123: 4500-4522.
- Rowan C.J. & Roberts A.P. 2006. Magnetite dissolution, diachronous greigite formation, and secondary magnetizations from pyrite oxidation: Unravelling complex magnetizations in Neogene marine sediments from New Zealand. *Earth and Planetary Science Letters* 241: 119-137.
- Sagnotti L. & Winkler A. 1999. Rock magnetism and palaeomagnetism of greigite-bearing mudstones in the Italian peninsula. *Earth and Planetary Science Letters* 165: 67-80.
- Snowball I.F. 1997a. Gyroremanent magnetization and the magnetic properties of greigite-bearing clays in southern Sweden. *Geophysical Journal International* 129: 624-636.
- Snowball I.F. 1997b. The detection of single-domain greigite (Fe<sub>3</sub>S<sub>4</sub>) using rotational remanent magnetization (RRM) and the effective gyro field (Bg): mineral magnetic and palaeomagnetic applications. *Geophysical Journal International* 130: 704-716.
- Sohlenius G. 1996. Mineral magnetic properties of Late Weichselian-Holocene sediments from the northwestern Baltic Proper. *Boreas* 25: 79-88.
- Sohlenius G., Sternbeck J., Andrén E. & Westman P. 1996. Holocene history of the Baltic Sea as recorded in a sediment core from the Gotland Deep. *Marine Geology* 134: 183-201.
- Sohlenius G., Emeis K.C., Andrén E., Andrén T. & Kohly A. 2001. Development of anoxia during the Holocene fresh-brackish water transition in the Baltic Sea. *Marine Geology* 177: 221-242.
- Stephenson A. 1980a. A gyroremanent magnetisation in anisotropic magnetic material. *Nature* 284: 49-51.
- Stephenson A. 1980b. Gyromagnetism and the remanence acquired by a rotating rock in an alternating-field *Nature* 284: 48-49.
- Stober J.C. & Thompson R. 1979a. An investigation into the source of magnetic minerals in some Finnish lake sediments. *Earth and Planetary Science Letters* 45: 464-474.
- Stober J.C. & Thompson R. 1979b. Magnetic remanence acquisition in Finnish lake sediments. *Geophysical Journal International* 57: 727-739.
- Stroeven A.P., Hättestrand C., Kleman J., Heyman J., Fabel D., Fredin O., Goodfellow B.W., Harbor J.M., Jansen J.D. & Olsen L. 2016. Deglaciation of fennoscandia. *Quaternary Science Reviews* 147: 91-121.
- Tikkanen P., Palonen V., Jungner H. & Keinonen J. 2004. AMS facility at the University of Helsinki. *Nuclear Instruments and Methods in Physics Research Section B: Beam Interactions with Materials and Atoms* 223: 35-39.
- Tuovinen N., Virtasalo J.J. & Kotilainen A.T. 2008. Holocene diatom stratigraphy in the Archipelago Sea, north-

- ern Baltic Sea. *Journal of Paleolimnology* 40: 793-807.
- van Helmond N.A.G.M., Krupinski N.B.Q., Lougheed B.C., Obrochta S.P., Andrén T. & Slomp C.P. 2017. Seasonal hypoxia was a natural feature of the coastal zone in the Little Belt, Denmark, during the past 8 ka. *Marine Geology* 387: 45-57.
- Vigouroux G., Kari E., Beltran-Abaunza J.M., Uotila P., Yuan D.K. & Destouni G. 2021. Trend correlations for coastal eutrophication and its main local and whole-sea drivers-Application to the Baltic Sea. *Science of the Total Environment* 779: 12.
- Virtasalo J.J., Kotilainen A.T., Räsänen M.E. & Ojala A.E.K. 2007. Late-glacial and post-glacial deposition in a large, low relief, epicontinental basin: the northern Baltic Sea. *Sedimentology* 54: 1323-1344.
- Virtasalo J.J., Endler M., Moros M., Jokinen S.A., Hämäläinen J. & Kotilainen A.T. 2016. Base of brackish-water mud as key regional stratigraphic marker of mid-Holocene marine flooding of the Baltic Sea Basin. *Geo-Marine Letters* 36: 445-456.
- Vuorela A., Lahdenperä A.-M., Penttinen T. & Posiva. 2009. *Review of Bothnian Sea shore-level displacement data and use of a GIS tool to estimate isostatic uplift*. Working report / Posiva, Posiva, Olkiluoto.
- Wang L., Pan Y.X., Li J.H. & Qin H.F. 2008. Magnetic properties related to thermal treatment of pyrite. *Science in China Series D-Earth Sciences* 51: 1144-1153.
- Warnock J.P., Bauersachs T., Kotthoff U., Brandt H.T. & Andrén E. 2018. Holocene environmental history of the Angermanälven Estuary, northern Baltic Sea. *Boreas* 47: 593-608.
- Winterhalter B. 1992. Late-Quaternary stratigraphy of Baltic Sea basins—a review. *Bulletin of the Geological Society of Finland* 64: 189-194.
- Zillén L., Conley D.J., Andrén T., Andrén E. & Björck S. 2008. Past occurrences of hypoxia in the Baltic Sea and the role of climate variability, environmental change and human impact. *Earth-Science Reviews* 91: 77-92.